Journal of
Materials Chemistry B

Materials for biology and medicine

rsc.li/materials-b

ROYAL SOCIETY
OF CHEMISTRY

PAPER
M. Melucci, V. Palermo *et al.*
Biomimetic graphene for enhanced interaction with the external
membrane of astrocytes

Biomimetic graphene for enhanced interaction with the external membrane of astrocytes†

M. Durso,‡[a] A. I. Borrachero-Conejo,‡[b] C. Bettini,[a] E. Treossi,[a] A. Scidà,[a] E. Saracino,[a] M. Gazzano,[a] M. Christian, [c] V. Morandi,[c] G. Tuci,[d] G. Giambastiani, [de] L. Ottaviano,[fg] F. Perrozzi,[g] V. Benfenati, [a] M. Melucci *[a] and V. Palermo*[ah]

Graphene and graphene substrates display huge potential as material interfaces for devices and biomedical tools targeting the modulation or recovery of brain functionality. However, to be considered reliable neural interfaces, graphene-derived substrates should properly interact with astrocytes, favoring their growth and avoiding adverse gliotic reactions. Indeed, astrocytes are the most abundant cells in the human brain and they have a crucial physiological role to maintain its homeostasis and modulate synaptic transmission. In this work, we describe a new strategy based on the chemical modification of graphene oxide (GO) with a synthetic phospholipid (PL) to improve interaction of GO with brain astroglial cells. The PL moieties were grafted on GO sheets through polymeric brushes obtained by atom-transfer radical-polymerization (ATRP) between acryloyl-modified PL and GO nanosheets modified with a bromide initiator. The adhesion of primary rat cortical astrocytes on GO–PL substrates increased by about three times with respect to that on glass substrates coated with standard adhesion agents (*i.e.* poly-D-lysine, PDL) as well as with respect to that on non-functionalized GO. Moreover, we show that astrocytes seeded on GO–PL did not display significant gliotic reactivity, indicating that the material interface did not cause a detrimental inflammatory reaction when interacting with astroglial cells. Our results indicate that the reported biomimetic approach could be applied to neural prosthesis to improve cell colonization and avoid glial scar formation in brain implants. Additionally, improved adhesion could be extremely relevant in devices targeting neural cell sensing/modulation of physiological activity.

[a] Consiglio Nazionale delle Ricerche, Istituto per la Sintesi Organica e la Fotoreattività (CNR-ISOF), via Piero Gobetti 101, 40129 Bologna, Italy. E-mail: manuela.melucci@isof.cnr.it, vincenzo.palermo@isof.cnr.it

[b] Consiglio Nazionale delle Ricerche, Istituto per lo Studio dei Materiali Nanostrutturati (CNR-ISMN), via Piero Gobetti 101, 40129 Bologna, Italy

[c] Consiglio Nazionale delle Ricerche, Istituto di Microelettronica e Microsistemi (IMM-CNR), via Piero Gobetti 101, 40129 Bologna, Italy

[d] Consiglio Nazionale delle Ricerche, Istituto di Chimica dei Composti Organometallici (ICCOM-CNR), Via Madonna del Piano 10, 50019 Sesto F.no (Firenze), Italy

[e] Kazan Federal University, 420008 Kazan, Russian Federation

[f] Dipartimento di Scienze Fisiche e Chimiche (DSFC), Università degli Studi dell'Aquila, via Vetoio 10, 67100 L'Aquila, Italy

[g] Consiglio Nazionale delle Ricerche, Istituto Superconduttori, Materiali innovativi e Dispositivi (CNR-SPIN Uos), via Vetoio 10, 67100 L'Aquila, Italy

[h] Chalmers University of Technology, Industrial and Materials Science, Hörsalsvägen 7A, SE-412 96 Goteborg, Sweden

† Electronic supplementary information (ESI) available: Synthetic and characterization of compounds **1–4** and GOBr, contact angles and XPS analysis details. See DOI: 10.1039/c8tb01410h

‡ These authors contributed equally to this work.

1. Introduction

Enhanced control of the interaction between nano-materials and living cells is becoming more and more important to allow future breakthroughs in different fields such as pharmacology, toxicology, bio-electronics and drug delivery. Nano-materials can interact strongly with different parts of the mammalian cell[1] but the first and most prominent interaction is usually with the cell membrane,[2] formed in almost all living organisms by a 2-dimensional, self-assembled layer of phospholipids (PLs). The PLs feature hydrophilic heads and long, flexible hydrophobic chains, whose supramolecular self-assembly drives the formation of the flexible and robust 2-dimensional membrane. PLs play a crucial role in intracellular signalling and participate in the regulation of cell growth, metabolism, differentiation, apoptosis, membrane trafficking, and cytoskeleton rearrangement. Chemical functionalization can be used to enhance the affinity of nanomaterials with cells, and PL-functionalized nanomaterials (*e.g.* carbon nanotubes or CdSe quantum dots) have already been proposed for studying PL signalling pathways, and employed as composites for drug delivery or biosensor applications.[3–8]

This journal is © The Royal Society of Chemistry 2018

J. Mater. Chem. B, 2018, **6**, 5335–5342 | 5335

In particular, biomaterials targeting the nervous system should interact properly with excitable neuronal cells but also with non-neuronal cells, called glial cells.[9] Indeed, astrocytes, that are the most numerous glial cells in the brain, have a crucial physiological role to maintain the homeostasis of the nervous system and modulate synaptic transmission. More importantly, brain injuries due to implantation of neural prostheses trigger an inflammatory response called reactive gliosis in which astrocytes are a major counterpart.[10] During astrogliosis cells suffer a dramatic morphological alteration (stellation), hypertrophy, trophic factor release and overexpression of structural proteins such as glial fibrillary acidic protein (GFAP). This process ultimately leads to the formation of a fibrous scar called glial scar, surrounding and insulating the implanted device with a thickness of hundreds of micrometers. Glial scar severely compromises the biomaterial/device performance, hinders neuronal regeneration and could also initiate detrimental processes leading to neuronal death.[11,12] Thus, the design and synthesis of materials capable of improving the adhesion of astrocytes without altering their morphology and physiology and without promoting this inflammatory response are needed for neural engineering and neuroregenerative medicine. Moreover, recent evidence increasingly indicates that astrocytes play an active role in the delivery/transduction/propagation of electrical stimulus to the central nervous system.[9] In this respect, even though they are not able to make action potentials, membrane channels and proteins of astrocytes are essential for brain functionality. Thus, it is essential to generate a novel interface that displays a tight interaction between the astrocytes' plasma membrane and the nanomaterial, allowing astrocyte adhesion, growth and permissive interplay with the material.

A single sheet of graphene or graphene oxide (GO) could be the ideal material to interact with the brain cells' membrane, thanks to its 2-dimensional shape, flexibility, mechanical strength and, more importantly, tuneable surface chemistry.[13a] Nowadays several nano-materials such as graphene, MoS_2 or carbon nanotubes can be processed in different solvents and deposited as thin coatings on a substrate.[13] However, their processing requires the use of toxic solvents, or significant amounts of surfactant molecules. Furthermore, the exfoliation of 2D materials always yields nanosheets with varying thickness, from monolayers to few nm, with lateral size typically <1 μm. Among 2D materials, GO is the only one that can be mass-produced in water, with no need for surfactants, in the form of monoatomic sheets with (tunable) lateral size from 100 μm to 100 nm, as we demonstrated in previous works.[14,15] Its highly versatile chemistry allows its chemical, electronic and optical properties to be tuned to an extent still unreachable for other 2D materials.[16–18]

Recent results from us and other groups have highlighted that graphene derivatives can have strong and specific interactions with cell membranes, with a parallel arrangement of the graphene sheets on the cellular surface.[19,20]

In light of their mechanical and chemophysical properties, the interaction of graphene-based materials such as flakes, sheets and films with neuronal cells has previously been investigated[21–25] for different purposes such as drug delivery systems targeted to brain cells,[24] coating films in conductive supports/scaffolds for neuroregenerative medicine,[26] neural interfaces, and transistors and electrode devices to monitor/manipulate the functionality of the nervous tissue.[27–29a] In this context, as the interaction between graphene nanomaterials and neural cells could drive intracellular changes due to their association with cell membranes, Prato, Ballerini and coworkers,[24] investigated whether exposure to 2D GO nanosheets could alter neuronal cell membrane-based processes, such as synaptic communication in both primary hippocampal neurons and cortical glial cultures. They found that GO nanosheets do not alter glial cell viability, nor synaptic communication. However, other authors found that graphene oxide nanosheets disrupt lipid composition of neuronal membranes and in turn alter Ca^{2+} homeostasis, and synaptic transmission of neuronal cells.[23]

The latter findings further motivate us to explore the use of phospholipids (PL) as interfacing molecules to functionalize graphene membranes targeting glial cells.

With this objective, here we describe a new type of GO composite specifically designed and synthesized for enhancing GO interaction with primary rat cortical astrocytes. We grafted PL moieties to GO sheets (Fig. 1) to get a biomimetic GO–PL composite capable of interacting with the cell membrane, fostering the adhesion and permissive interaction with astrocytes on the target substrate. Indeed, despite their importance on brain physiology and pathology, with respect to neurons, the interaction of astrocytes with chemically modified graphene materials has received much lower attention.[29b,c] Interestingly, electrospun PCL microfiber scaffolds coated with graphene polyelectrolyte multilayer suppress microglia and astrocytes gliotic activation after implantation *in vivo*. Thermally modified graphene nanosheets do not have a deleterious effect on the resident neuron and astrocyte populations of the olfactory bulb *in vivo*.[29c] Collectively, these evidence indicated that modified GO is a permissive material for both neurons and astrocytes.

A molecule tethered to a mesoscopic GO nanosheet can be considered neither free floating in solution, nor grafted to a macroscopic, rigid bulk substrate; it is rather in a condition halfway between these two.[30] Molecules may be tethered to GO
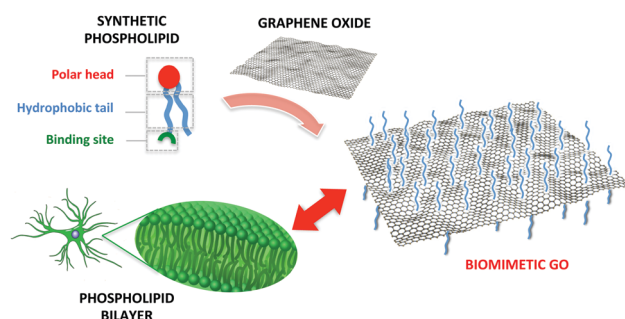

Fig. 1 Sketch of the rationale of this work. A synthetic phospholipid is tailored to bind to graphene oxide with the aim of enhancing the interactions with cell membranes.

sheets without perturbing their chemical and optical properties, by choosing the right covalent linkers.[16]

Thus, a key step to maximize the interaction of our material with cells was to give a high conformational degree of freedom to the PL grafted on GO nanosheets, ensuring that PL molecules could rearrange in the best way to interact effectively with the lipid bilayer. To this aim we use a flexible polymeric linker to graft the PL moiety through one of the apolar tail leaving 'free' both polar head and an apolar tails. All the PEG-modified phospholipids commercially available bear the reactive functional groups on their head, thus enabling the PL tethering on the GO surface only by the polar head.

Therefore we used a synthetic procedure to position the reactive functional moiety (an acryloyl group) on one of the tails of the phospholipid (Fig. 1). Then Atom-Transfer Radical-Polymerization (ATRP) was exploited for the covalent grafting of PL on GO through flexible brush linkers.

The PL-modified GO obtained was processed in flat membranes that were used as astrocyte-culturing substrates. Comparison with unmodified GO and reduced rGO membranes prepared in the same way was also performed to provide an insight into the actual role of the PL modification.

2. Materials and methods

2.1 Synthesis and characterization

1,12-Dodecanediol, acryloyl chloride, pyridine, pyridinium dichromate, 4-dimethyl aminopyridin (DMAP), N,N'-dicyclohexyl-carbodiimide, triethylamine (TEA), and α-bromoisobutyryl bromide were purchased in the highest grade available from Sigma-Aldrich Co, Milan, Italy and were used without further purification. 1-Palmitoyl-2-hydroxy-sn-glycero-3-phosphocholine (3) was purchased from AVANTI POLAR LIPIDS, inc. All ^{1}H NMR and ^{13}C NMR spectra were recorded at room temperature on a Varian Mercury-400 spectrometer (Varian, Palo, Alto, CA, USA) equipped with a 5 mm probe. The synthesis of 12-(acryloyloxy)-1-dodecanol (1), 12-(acryloyloxy)-1-dodecanoic acid (2). 1-Palmitoyl-2-[12-(acryloyloxy)dodecanoyl]-sn-glycero-3-phosphocholine (4) and GOBr precursors are reported in the ESI.†

GO–PL. GO-Br (50 mg), 1-palmitoyl-2-[12-(acryloyloxy)-dodecanoyl]-sn-glycero-3-phosphocholine 4, (20 mg), CuBr (1 mg), bipyridine (2 mg) and a small piece of copper(0) wire were placed into a round bottom flask. The flask was degassed and 6 mL of degassed MeOH were added. The mixture was stirred at 35 °C for 48 h, then diluted with ethanol and centrifuged for 40′ at 14 000 rpm. The supernatant was removed and the washing cycle was repeated two times with ethanol and then three times with chloroform. Part of the product was dried under vacuum to obtain about 50 mg of a dark grey powder. Part of the product was kept as a solution in chloroform (c = 2 mg mL^{-1}). Elemental analysis: N% = 2.16, C% = 42.51, H% = 2.94, S% = 0.57.

2.2 Fabrication of membranes

GO and GO–PL membranes were fabricated by filtration of GO or GO–PL dispersions through an AnodiscTM membrane filter (Whatman, 47 mm in diameter, 0.2 μm pore size), followed by air drying and peeling from the filter. The rGO membrane was prepared by annealing of a GO membrane at 200 °C for one hour under vacuum.[18,31,32] The weight of the GO, rGO and GO–PL membranes was around 15 mg and the diameter was ≈3.7 cm.

2.3 Preparation of primary astroglia rat culture

Primary astroglia cortical cultures were prepared from rats as described in the literature.[33] One to two days old Sprague Dawley pups were taken and the cerebral cortices were removed, mechanically dissociated and placed in cell culture flasks containing DMEM-Glutamax medium supplemented with 15% fetal bovine serum (FBS), 100 U mL^{-1} penicillin and 100 mg mL^{-1} streptomycin. Cells were maintained in incubation at 37 °C and 5% CO$_2$ with the proper humidity levels for three to four weeks. The medium was changed every three days and the flasks were gently shaken to detach undesired cells that remained on top of the astrocytic monolayer. Cells were finally seeded for experiments and maintained in a culture medium containing 10% FBS. Primary astroglial cultures were prepared at the University of Bologna and performed in concordance with the Italian law of protection of laboratory animals (ethical protocol number no. 360/2017 PR).

2.4 Biocompatibility study

Fluorescein diacetate (FDA) was used as a marker of viable cells to take pictures. The FDA stock solution (5 mg mL^{-1}) was diluted on phosphate buffered saline (PBS). Astrocytes plated on the substrates were incubated for 5 min at RT, washed with PBS and characterized by (Nikon eclipse 80i) microscope equipped with a 20× objective.

Alamar blue (AB, Life Technologies) viability assay was used according to the manufacturer's protocol to study the viability of cells on the device at different time points. Alamar blue assay (ABA) is a cell viability indicator. It takes advantage of the reducing power of living cells to quantitatively measure the cell number and the proliferation rate of living cells. Moreover, ABA takes advantage of the reduction occurring in the cytoplasm of living cells by enzymatic activity related to aerobic respiration providing even non-specific information on cell metabolism.[33] Cells plated on the GO, rGO and GO–PL samples and glass + PDL control were incubated at 37 °C for 6 h with AB that was diluted in an amount equal to 10% of the culture volume. After that 100 μL were taken and then placed into a 96 well plate for fluorescence measurements in a Thermo Scientific™ Varioskan™ Flash Multimode Reader at an emission and excitation wavelength of 585 nm and 570 nm respectively.

Proliferation rate was calculated as the increase in fluorescence, which is proportional to the number of cells, between two successive days and it was expressed as a percentage. It was calculated for 2 and 4 DIV. All the experiments were performed three times in triplicate.

2.5 Immunofluorescence and confocal microscopy

Mouse anti-GFAP (Sigma Aldrich, Milan, Italy) diluted to 1 : 300 was used as the primary antibody. The secondary antibody used

This journal is © The Royal Society of Chemistry 2018

J. Mater. Chem. B, 2018, 6, 5335–5342 | 5337

was Alexa 488-conjugated goat anti-mouse at a dilution of 1:1000. Cultured astrocytes plated on the samples were fixed in 4% paraformaldehyde, and washed in phosphate buffered saline (PBS). After blocking with 3% BSA in PBS and permeabilizing with 0.1% Triton X-100 in PBS, cells were incubated with primary antibodies for 3 h at RT, washed in PBS and incubated for 1 h at RT with the secondary antibody. Coverslips were mounted on slides, using ProLong Diamond Antifade Mountant with DAPI and examined with a Nikon TE 2000 inverted confocal microscope equipped with a $40\times$ objective and a 400 nm diode, 488 nm Ar^+ and 543 nm He–Ne lasers as exciting sources.

2.6 Image processing and analysis

Image processing and analysis was performed using the FIJI distribution of ImageJ with a custom processing script.[34] Briefly, images from the confocal imaging software (Nikon EZ-C1 2.10) were imported into ImageJ, cropped and converted to greyscale TIFF format images. Manual thresholding was applied to generate a binary mask to separate cellular fluorescence from the background. This mask was eroded, dilated, and used to generate a region of interest (ROI) encompassing all of the cells present in the image. An inverted version of the previous binary mask was used to identify a ROI for the image background.

The mean fluorescence, ROI area, and integrated density values for the cellular fluorescence and background were measured for each image. These values were used to calculate the corrected total cell fluorescence according to previously published works.[35,36] Corrected total cellular fluorescence was calculated and reported as an average of four fields of view for each of the four substrate conditions, for a total of 16 images.

2.7 Statistical analyses

Results are represented as the mean $\pm$ Standard Error (SE) from at least three independent experiments performed in triplicate. Data were compared by one-way ANOVA with Bonferroni *post hoc* test. Statistically significant difference was reported if $p < 0.05$.
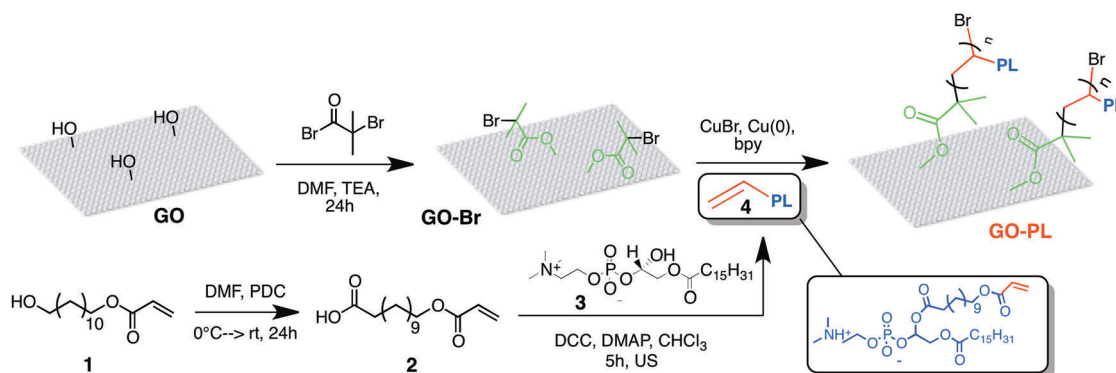
3. Results and discussion

3.1 Design, synthesis and characterization

The covalent grafting of PL on GO nanosheets was achieved by ATRP between the acryloyl-modified PL and GO nanosheets modified with a bromide initiator, an approach successfully used in the literature for the covalent modification of silica surfaces with PL-brushes.[37–40]

GO–PL was thus prepared through a multi-step synthetic approach as outlined in Scheme 1.

The ATRP reaction was carried out in degassed MeOH as solvent and catalysed by Cu(ɪ)Br/2,2′-bipyridine (bpy). Copper(0) addition was also required for successful reaction.[40b] X-Ray Diffraction (XRD), Fourier Transform Infrared (FTIR), elemental analysis and X-ray Photoelectron Spectroscopy (XPS) confirmed the successful functionalization (Fig. 2 and 3). The powder XRD diffractogram of GO–PL and that of the reference GO are shown in Fig. 2a. Pristine GO showed a typical stacking periodicity of 0.75 nm, in good agreement with previously reported data from the literature.[31,41] GO–PL showed a much larger stacking, with a periodicity of 1.25 nm, indicating the presence of a 0.5 nm thick interlayer present between GO sheets. Such a thickness matches well with the expected phospholipid structure. Scanning Electron Microscopy (SEM) images of GO–PL showed a typical graphene-like structure, with highly anisotropic, flexible sheets featuring a lateral size of a few μm and a significant tendency to stack on each other (Fig. 2b). FTIR spectra of GO–PL, GO initiator and PL are shown in Fig. 2c. The typical bands of C–H stretching in the range of 2850–2950 cm^{-1} are evident as well as the C=O stretching at about 1730 cm^{-1}. Also P–O and P=O stretching are present in the composite (850–1200 cm^{-1}). The same features of PL are preserved in the spectrum of GO–PL. On the other hand, the GO-initiator spectrum shows the C–Br stretching at about 500–700 cm^{-1}, preserved also in part in the composite spectrum. The XPS analysis (Fig. 3) confirms the presence of nitrogen and phosphorus in 4 and 2 at% respectively, in good accordance with outcomes from elemental analysis (N 2.16, C 42.51, H 2.94). The N:P ratio of 2:1 can be reasonably ascribed to material contamination from solvents (*i.e.* DMF and/or Et_3N) used for the synthesis of the GO–Br precursor (XPS analysis on GO-Br already shows 2 N at%) that are not removed during the material work-up

Scheme 1 Synthetic route to GO–PL.

5338 | *J. Mater. Chem. B,* 2018, **6**, 5335–5342

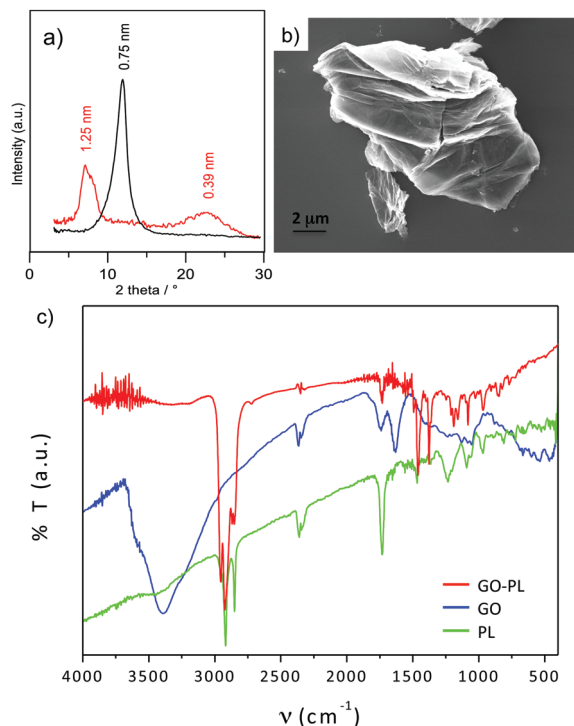This journal is © The Royal Society of Chemistry 2018

Fig. 2 (a) Diffractograms of GO (black line) and GO−PL (red line), the baseline was subtracted to enhance peaks. (b) SEM image of a GO−PL flake, (c) FTIR spectra of GO (blue line), PL (green line) and GO−PL (red line).
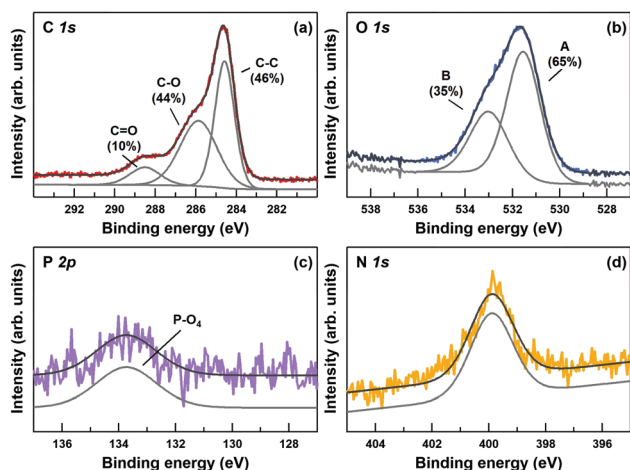

Fig. 3 Core level spectra of C 1s (a), O 1s (b), P 2p (c) and N 1s (d).

(drying is carried out at room temperature to avoid material decomposition and loss of covalently grafted groups). In fact, traces of solvent(s) are maintained in the final GO−PL. Nevertheless, the amount of P (2 at%) allows a loading of about 1.2 mmol of PL per g of material to be estimated. Finally, taking into account the 1:2 P:Br ratio (Br = 4 at%), it can be inferred that only half of the bromine groups in the GO-Br initiator have been reacted with PL. Furthermore a C/O ratio of 2.6 was calculated from the XPS analysis. This value is in accord with the expected GO−PL composite, since the C/O ratio of GO is typically close to 2.0[13b] while the C/O ratio of PL is 3.8.

3.2 Membrane fabrication and characterization

GO and GO–PL substrates were fabricated by filtration of water suspensions through an Anodisc™ membrane filter, followed by slow drying in air. This procedure allowed uniform, thin substrates to be obtained, conventionally called "GO paper" (Fig. 4a), where the sheets were tightly packed on each other (Fig. 4b and c).

The as-prepared substrates were both mechanically and chemically stable and they could be easily detached from the filter support and handled for their final application.

A strong difference in surface roughness (R_a) between GO–PL (R_a = 550 ± 130 nm) and its pristine GO counterpart (R_a = 170 nm ± 50 nm) was measured by profilometry. Such a difference was likely due to the different stacking of the two materials, already evident by XRD (Fig. 2a). Contact angle measurements (Fig. 4d–f, details in ESI†)[32] demonstrated higher hydrophobicity for GO–PL with respect to GO. This result could be likely due to the presence of the aliphatic polymeric brush linkers on GO surface. Moreover, the higher hydrophobicity also suggests that PL moieties are arranged in such a way that they do not expose the polar head to the outer membrane surface.

3.3 GO–PL promotes cell adhesion without inducing gliosis

The biocompatibility of the as-prepared GO–PL was then studied by using them as a substrate to grow primary rat astroglial cells. For the sake of comparison, we also used state-of-the-art glass
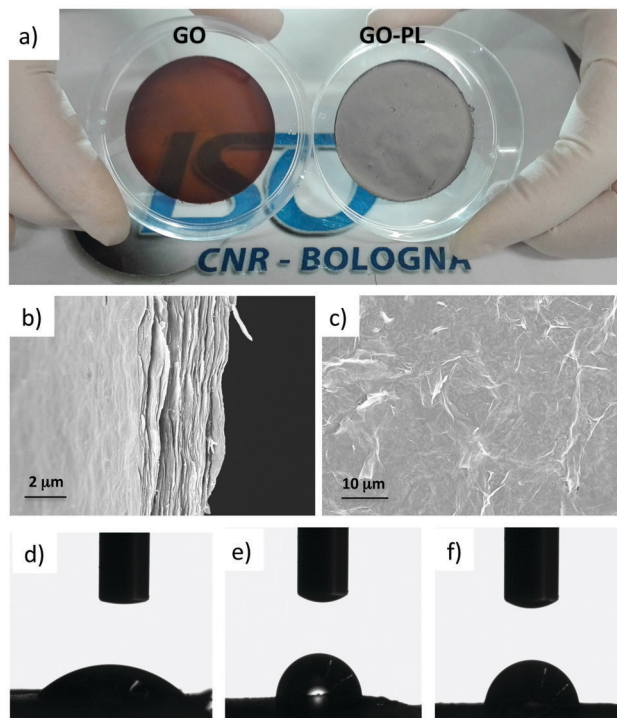

Fig. 4 (a) Images of GO and GO−PL membranes. (b and c) SEM image of the cross section and top view of GO−PL, (d−f) shapes of a water droplet (1 μL) on the surface of a GO ((d) 41 ± 1°) rGO ((e) 86 ± 1.68°) and GO−PL ((f) 78 ± 1°).
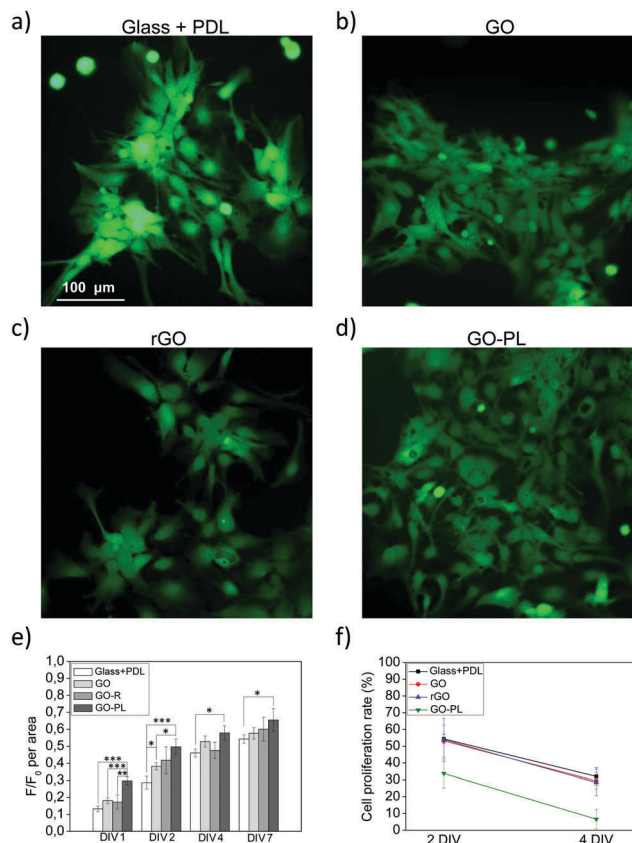
Fig. 5 Biocompatibility study of GO, rGO and GO–PL. (a–d) Representative micrographs of FDA stained astrocytes plated on glass + PDL as reference, GO, rGO and GO–PL taken at 2 DIV. (e) Histogram plot shows averaged F/F_0 per area plated on GLASS + PDL ($n = 18$), GO ($n = 17$), rGO ($n = 9$) and GO–PL ($n = 18$), after 1, 2, 4 and 7 DIV. (*$p < 0.05$; **$p < 0.01$; ***$p < 0.001$, One-way ANOVA). Results represent at least three independent experiments. (f) Cell proliferation on the 4 substrates at DIV2 and DIV 4, calculated as indicated in materials and methods. The slope of the curve is identical, indicating that the proliferation rate was comparable for all substrates.
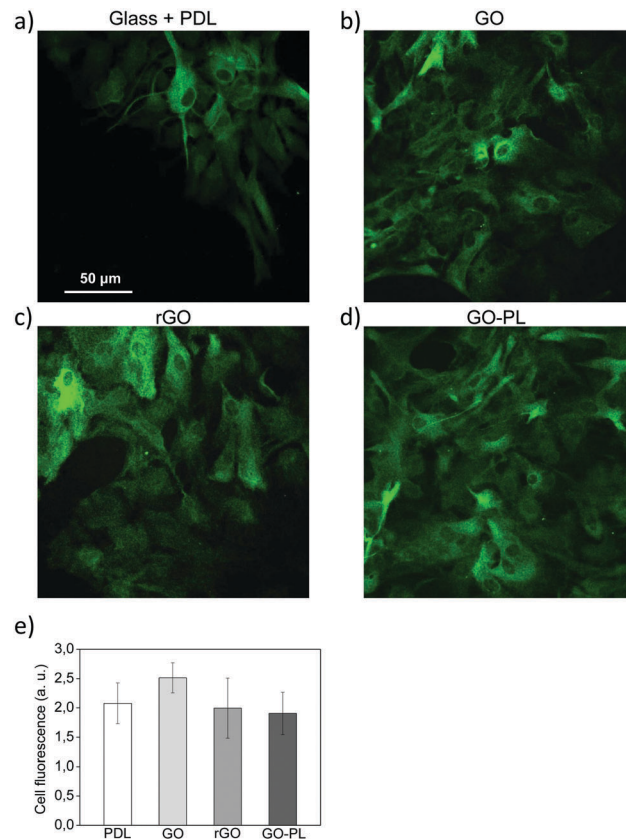

Fig. 6 GFAP protein expression in astrocytes plated on PDL, GO, rGO and GO–PL. (a–d) Confocal imaging of astrocytes stained with GFAP. (e) Quantification of GFAP immunofluorescent signal. The analyses revealed that the immunofluorescent signal was comparable among different samples.

substrates treated with conventional coatings of poly-D-lysine (PDL), as well as non-functionalized, pristine GO and rGO. Astrocytes were then plated on GO–PL, GO, rGO and glass + PDL substrates. Fluorescein diacetate (FDA) assay and fluorescent microscopy were performed after 2 days *in vitro* (DIV) as shown in the micrographs in Fig. 5a–d. Viable cells stained with FDA (green) were visible on all four substrates.[26,27] Interestingly, the number of viable cells appeared higher on GO–PL samples than on glass or GO substrates. To get a more quantitative comparison of cell viability among the different conditions tested, an Alamar blue cell viability assay was performed after 1, 2, 4 and 7 DIV (Fig. 5e). The histogram plots reported in Fig. 5e show the F/F_0 ratio per area, which is directly proportional to the number of viable cells per sample.[42] The number of astrocytes that adhered to GO and rGO was comparable to those adhering to glass + PDL, while the adhesion of astrocytes to GO–PL was more than doubled at 1 DIV and also significantly higher for 2, 4 and 7 DIV. The higher number of cells observed on GO–PL could not be due to a hypertrophic or gliotic response. Indeed, the proliferation rate was

comparable among all samples observed (Fig. 5f). Thus, the higher number of cells in GO–PL observed at 1 DIV and 2 DIV could be explained by the higher adhesion of astrocytes on GO–PL. The area available for cell adhesion was the same for all the samples; thus, confluence (occupancy of all available space) and contact inhibition of proliferation occurred earlier in cells grown on GO–PL than in cells plated on the reference samples. For higher DIV, this also caused the lower cell proliferation (in percentage) observed on GO–PL *vs.* other samples (Fig. 5e).

The significantly lower number of cells that adhere to rGO when compared with GO–PL indicates that higher adhesion of astrocytes on GO–PL is not due to a difference in roughness or hydrophobicity as both substrates present very similar values for these properties.

Comparable surface properties in terms of roughness and hydrophobicity between rGO and GO–PL suggest that surface chemistry might account for the higher astrocyte adhesion on GO–PL. Moreover, despite further insight is required to highlight the mechanism of interaction between GO–PL and cell membrane, the higher hydrophobicity of GO–PL suggests that the polar heads of the PL moieties are not exposed to the outer surface indicating possible interaction GO–PL/cell membrane through the aliphatic apolar tails.

Finally, we looked for any evidence of gliotic reaction possibly triggered by GO, rGO and GO–PL samples. With this aim, we evaluated the expression of GFAP (Glial Fibrillary Acidic Protein), a well-known marker of astrogliosis *in vitro* and *in vivo*.[43] We performed confocal imaging on astrocytes grown on glass + PDL, GO, rGO and GO–PL after immuno-fluorescent staining of GFAP (Fig. 6a–d). Immunofluorescent imaging and quantitative analyses of the fluorescent signal (Fig. 6e) confirmed that the levels of GFAP expressed were similar for cells grown on all the different substrates, thus suggesting that GO, rGO and GO–PL did not promote gliotic reaction *in vitro*.

4. Conclusions

Taken together, the reported data suggest that PL-modified GO showed a significant enhancement in the adhesion of astrocytes with respect to GO, rGO or glass substrates coated with poly-D-lysine, without promoting a gliotic reaction, and this enhancement could not be ascribed to physical properties of the substrates. Our results indicate that GO–PL coatings deposited from solution could be a versatile, tuneable and effective coating for interfacing neural cells of glial origin and prepare the pathway for innovative brain material interfaces.

Conflicts of interest

There are no conflicts to declare.

Acknowledgements

Notes and references

1 J. Liu, L. Cui and D. Losic, *Acta Biomater.*, 2013, **9**, 9243–9257.

2 Y. Tu, M. Lv, P. Xiu, T. Huynh, M. Zhang, M. Castelli, Z. Liu, Q. Huang, C. Fan, H. Fang and R. Zhou, *Nat. Nanotechnol.*, 2013, **8**, 594–601.

3 D. Tan, L. Liu, Z. Li and Q. Fu, *J. Biomed. Mater. Res., Part A*, 2015, **103**, 2711–2719.

4 C. Thauvin, S. Rickling, P. Schultz, H. Célia, S. Meunier and C. Mioskowski, *Nat. Nanotechnol.*, 2008, **3**, 743–748.

5 C. Richard, F. Balavoine, P. Schultz, T. W. Ebbesen and C. Mioskowski, *Science*, 2003, **300**, 775–779.

6 G. Gopalakrishnan, C. Danelon, P. Izewska, M. Prummer, P. Y. Bolinger, I. Geissbühler, D. Demurtas, J. Dubochet and H. Vogel, *Angew. Chem., Int. Ed.*, 2006, **45**, 5478–5483.

7 D. Li, G. P. Li, P. C. Li, L. X. Zhang, Z. J. Liu, J. Wang and E. K. Wang, *Biomaterials*, 2010, **31**, 1850–1857.

8 C. Cheng, S. Li, A. Thomas, N. A. Kotov and R. Haag, *Chem. Rev.*, 2017, **117**, 1826–1914.

9 J. W. Salatino, K. A. Ludwig, T. D. Y. Kozai and E. K. Purcell, *Nat. Biomed. Eng.*, DOI: 10.1038/s41551-017-0154-1.

10 J. E. Burda and M. V. Sofroniew, *Neuron*, 2014, **81**, 229–248.

11 J. Silver and J. H. Miller, *Nat. Rev. Neurosci.*, 2004, **5**, 146–156.

12 J. W. Salatino, B. M. Winter, M. H. Drazin and E. K. Purcell, *J. Neurophysiol.*, 2017, **118**, 194–202.

13 (*a*) K. R. Paton, E. Varrla, C. Backes, R. J. Smith, U. Khan, A. O'Neill, C. Boland, M. Lotya, O. M. Istrate, P. King, T. Higgins, S. Barwich, P. May, P. Puczkarski, I. Ahmed, M. Moebius, H. Pettersson, E. Long, J. Coelho, S. E. O'Brien, E. K. McGuire, B. M. Sanchez, G. S. Duesberg, N. McEvoy, T. J. Pennycook, C. Downing, A. Crossley, V. Nicolosi and J. N. Coleman, *Nat. Mater.*, 2014, **13**, 624–630; (*b*) F. Perrozzi, S. Prezioso, M. Donarelli, F. Bisti, P. De Marco, S. Santucci, M. Nardone, E. Treossi, V. Palermo and L. Ottaviano, *J. Phys. Chem. C*, 2013, **117**, 620.

14 E. Treossi, M. Melucci, A. Liscio, M. Gazzano, P. Samorì and V. Palermo, *J. Am. Chem. Soc.*, 2009, **131**, 15576–15577.

15 A. Liscio, K. Kouroupis-Agalou, X. D. Betriu, A. Kovtun, E. Treossi, N. M. Pugno, G. De Luca, L. Giorgini and V. Palermo, *2D Mater.*, 2017, **4**, 25017.

16 M. Melucci, M. Durso, M. Zambianchi, E. Treossi, Z.-Y. Xia, I. Manet, G. Giambastiani, L. Ortolani, V. Morandi, F. De Angelis and V. Palermo, *J. Mater. Chem.*, 2012, **22**, 18237.

17 M. Melucci, E. Treossi, L. Ortolani, G. Giambastiani, V. Morandi, P. Klar, C. Casiraghi, P. Samorì and V. Palermo, *J. Mater. Chem.*, 2010, **20**, 9052.

18 A. Vianelli, A. Candini, E. Treossi, V. Palermo and M. Affronte, *Carbon*, 2015, **89**, 188–196.

19 M. Kucki, P. Rupper, C. Sarrieu, M. Melucci, E. Treossi, A. Schwarz, V. León, A. Kraegeloh, E. Flahaut, E. Vázquez, V. Palermo and P. Wick, *Nanoscale*, 2016, **8**, 8749–8760.

20 J. Russier, E. Treossi, A. Scarsi, F. Perrozzi, H. Dumortier, L. Ottaviano, M. Meneghetti, V. Palermo and A. Bianco, *Nanoscale*, 2013, **5**, 11234.

21 S. Marchesan, L. Ballerini and M. Prato, *Science*, 2017, **356**, 1010–1011.

22 Ç. Defterali, R. Verdejo, L. Peponi, E. D. Martín, R. Martínez-Murillo, M. Á. López-Manchado and C. Vicario-Abejón, *Biomaterials*, 2016, **82**, 84–93.

23 M. Bramini, S. Sacchetti, A. Armirotti, A. Rocchi, E. Vázquez, V. León Castellanos, T. Bandiera, F. Cesca and F. Benfenati, *ACS Nano*, 2016, **10**, 7154–7171.

24 R. Rauti, N. Lozano, V. León, D. Scaini, M. Musto, I. Rago, F. P. Ulloa Severino, A. Fabbro, L. Casalis, E. Vázquez, K. Kostarelos, M. Prato and L. Ballerini, *ACS Nano*, 2016, **10**, 4459–4471.

25 Q. Tu, L. Pang, Y. Chen, Y. R. Zhang, R. Zhang, B. Z. Lu and J. Y. Wang, *Analyst*, 2014, **139**, 105–115.

26 A. Domínguez-Bajo, A. González-Mayorga, E. López-Dolado and M. C. Serrano, *Front. Syst. Neurosci.*, 2017, DOI: 10.3389/fnsys.2017.00071.

27 T. Cohen-Karni, Q. Qing, Q. Li, Y. Fang and C. M. Lieber, *Nano Lett.*, 2010, **10**, 1098–1102.

28 F. Veliev, Z. Han, D. Kalita, A. Briançon-Marjollet, V. Bouchiat and C. Delacour, *Front. Neurosci.*, 2017, **11**, 1–11.

29 (*a*) N. Liu, A. Chortos, T. Lei, L. Jin, T. R. Kim, W. G. Bae, C. Zhu, S. Wang, R. Pfattner, X. Chen, R. Sinclair and Z. Bao, *Sci. Adv.*, 2017, **3**, 1–10; (*b*) K. Zhou, S. Motamed, G. A. Thouas, C. C. Bernard, D. Li, H. C. Parkington, H. A. Coleman, D. I. Finkelstein and J. S. Forsythe, *PLoS One*, 2016, **11**(3), e0151589; (*c*) C. Defteralı, R. Verdejo, I. Peponi, E. D. Martín, R. Martínez-Murillo, M. A. López-Manchado and C. Vicario-Abejón, *Biomaterials*, 2016, **82**, 84–93.

30 V. Palermo, *Chem. Commun.*, 2013, **49**, 2848.

31 A. Liscio, G. P. Veronese, E. Treossi, F. Suriano, F. Rossella, V. Bellani, R. Rizzoli, P. Samorì and V. Palermo, *J. Mater. Chem.*, 2011, **21**, 2924.

32 F. Perrozzi, S. Croce, E. Treossi, V. Palermo, S. Santucci, G. Fioravanti and L. Ottaviano, *Carbon*, 2014, **77**, 473–480.

33 A. Sagnella, A. Pistone, S. Bonetti, A. Donnadio, E. Saracino, M. Nocchetti, C. Dionigi, G. Ruani, M. Muccini, T. Posati, V. Benfenati and R. Zamboni, *RSC Adv.*, 2016, **6**, 9304–9314.

34 J. Schindelin, I. Arganda-Carreras, E. Frise, V. Kaynig, M. Longair, T. Pietzsch, S. Preibisch, C. Rueden, S. Saalfeld, B. Schmid, J. Y. Tinevez, D. J. White, V. Hartenstein, K. Eliceiri, P. Tomancak and A. Cardona, *Nat. Methods*, 2012, **9**, 676–682.

35 R. A. McCloy, S. Rogers, C. E. Caldon, T. Lorca, A. Castro and A. Burgess, *Cell Cycle*, 2014, **13**, 1400–1412.

36 A. Burgess, S. Vigneron, E. Brioudes, J.-C. Labbé, T. Lorca and A. Castro, *Proc. Natl. Acad. Sci. U. S. A.*, 2010, **107**, 12564–12569.

37 K. G. Marra, T. M. Winger, S. R. Hanson and E. L. Chaikof, *Macromolecules*, 1997, **9297**, 6483–6488.

38 R. Rosseto and J. Hajdu, *Tetrahedron*, 2005, **46**, 2941–2944.

39 S. H. Lee, D. R. Dreyer, J. H. An, A. Velamakanni, R. D. Piner, S. Park, Y. W. Zhu, S. O. Kim, C. W. Bielawski and R. S. Ruoff, *Macromol. Rapid Commun.*, 2010, **31**, 281–288.

40 (*a*) W. Feng, S. Zhu, K. Ishihara and J. L. Brash, *Langmuir*, 2005, **21**, 5980–5987; (*b*) C. Boyer, N. A. Corrigan, K. Jung, D. Nguyen, T.-K. Nguyen, N. N. M. Adnan, S. Oliver, S. Shanmugam and J. Yeow, *Chem. Rev.*, 2016, **116**, 1803–1949.

41 G. Romanelli, A. Liscio, R. Senesi, R. Zamboni, E. Treossi, F. Liscio, G. Giambastiani, V. Palermo, F. Fernandez-Alonso and C. Andreani, *Carbon*, 2016, **108**, 199–203.

42 T. Posati, A. Pistone, E. Saracino, F. Formaggio, M. G. Mola, E. Troni, A. Sagnella, M. Nocchetti, M. Barbalinardo, F. Valle, S. Bonetti, M. Caprini, G. P. Nicchia, R. Zamboni, M. Muccini and V. Benfenati, *Sci. Rep.*, 2016, **6**, 1–16.

43 L. F. Eng and R. S. Ghirnikar, *Brain Pathol.*, 1994, **4**, 229–237.